CANDIDATE RR LYRAE STARS FOUND IN SLOAN DIGITAL SKY SURVEY COMMISSIONING DATA[1]

Željko Ivezić,[2] Josh Goldston,[2] Kristian Finlator,[2] Gillian R. Knapp,[2] Brian Yanny,[3] Timothy A. McKay,[4] Susan Amrose,[4] Kevin Krisciunas,[5] Beth Willman,[5] Scott Anderson,[5] Chris Schaber,[5] Dawn Erb,[5] Chelsea Logan,[5] Chris Stubbs,[5] Bing Chen,[6] Eric Neilsen,[6] Alan Uomoto,[6] Jeffrey R. Pier,[7] Xiaohui Fan,[2] James E. Gunn,[2] Robert H. Lupton,[2] Constance M. Rockosi,[8] David Schlegel,[2] Michael A. Strauss,[2] James Annis,[3] Jon Brinkmann,[9] István Csabai,[6,10] Mamoru Doi,[11] Masataka Fukugita,[12,13] Gregory S. Hennessy,[14] Robert B. Hindsley,[15] Bruce Margon,[5] Jeffrey A. Munn,[7] Heidi Jo Newberg,[16] Donald P. Schneider,[17] J. Allyn Smith,[4] Gyula P. Szokoly,[18] Aniruddha R. Thakar,[6] Michael S. Vogeley,[2] Patrick Waddell,[5] Naoki Yasuda,[19] and Donald G. York[8]

FOR THE SDSS COLLABORATION

ABSTRACT

We present a sample of 148 candidate RR Lyrae stars selected from Sloan Digital Sky Survey (SDSS) commissioning data for about 100 deg² of sky surveyed twice with $\Delta t = 1.9946$ days. Although the faint-magnitude limit of the SDSS allows us to detect RR Lyrae stars to large Galactocentric distances (~ 100 kpc, or $r^* \sim 21$), we find no candidates fainter than $r^* \sim 20$, i.e., farther than ~ 65 kpc from the Galactic center. On the assumption that all 148 candidates are indeed RR Lyrae stars (contamination by other species of variable star is probably less than 10%), we find that their volume density has roughly a power-law dependence on Galactocentric radius, $R^{-2.7 \pm 0.2}$, between 10 and 50 kpc and drops abruptly at $R \sim 50$–60 kpc, possibly indicating a sharp edge to the stellar halo as traced by RR Lyrae stars. The Galactic distribution of stars in this sample is very inhomogeneous and shows a clump of over 70 stars at about 45 kpc from the Galactic center. This clump is also detected in the distribution of nonvariable objects with RR Lyrae star colors. When sources in the clump are excluded, the best power-law fit becomes consistent with the R^{-3} distribution found from surveys of bright RR Lyrae stars. These results imply that the halo contains clumpy overdensities inhomogeneously distributed within a smooth R^{-3} background, with a possible cutoff at ~ 50 kpc.

Key words: Galaxy: halo — Galaxy: stellar content — Galaxy: structure — RR Lyrae variable

1. INTRODUCTION

The Sloan Digital Sky Survey (SDSS) is a digital photometric and spectroscopic survey that will cover one-quarter of the celestial sphere in the north Galactic cap and produce a smaller area (~ 225 deg²) but much deeper survey in the southern Galactic hemisphere (Gunn & Weinberg 1995; York et al. 2000).[20] The flux densities of detected objects are measured almost simultaneously in five bands (u', g', r', i', and z'; Fukugita et al. 1996) with effective wavelengths of 3540, 4760, 6280, 7690, and 9250 Å, complete to limiting (5:1 signal-to-noise ratio) point-source magnitudes of 22.3, 23.3, 23.1, 22.3, and 20.8 in the north Galactic cap.[21] The survey sky coverage of about π sr will result in photometric measurements to the above detection limits for about 10^8 stars. The pixel size (0″.4) and optical quality of the telescope are such that the resolution is limited by atmospheric

---

[2] Princeton University Observatory, Peyton Hall, Princeton, NJ 08544-1001.
[3] Fermi National Accelerator Laboratory, P.O. Box 500, Batavia, IL 60510.
[4] Department of Physics, University of Michigan, 500 East University, Ann Arbor, MI 48109-1120.
[5] Department of Astronomy, University of Washington, Box 351580, Seattle, WA 98195.
[6] Department of Physics and Astronomy, Johns Hopkins University, 3400 North Charles Street, Baltimore, MD 21218-2686.
[7] US Naval Observatory, Flagstaff Station, P.O. Box 1149, Flagstaff, AZ 86002.
[8] Department of Astronomy and Astrophysics, University of Chicago, 5640 South Ellis Avenue, Chicago, IL 60637.
[9] Apache Point Observatory, P.O. Box 59, Sunspot, NM 88349.
[10] Department of Physics of Complex Systems, Eötvös University, Pázmány Péter sétány 1/A, H-1117 Budapest, Hungary.
[11] Department of Astronomy and Research Center for the Early Universe, School of Science, University of Tokyo, 7-3-1 Hongo, Bunkyo, Tokyo 113-0033, Japan.
[12] Institute for Cosmic Ray Research, University of Tokyo, 3-2-1 Midori, Tanashi, Tokyo 188-8502, Japan.
[13] Institute for Advanced Study, Olden Lane, Princeton, NJ 08540-0631.
[14] US Naval Observatory, 3450 Massachusetts Avenue, NW, Washington, DC 20392-5420.
[15] Remote Sensing Division, Code 7215, Naval Research Laboratory, 4555 Overlook Avenue, SW, Washington, DC 20375.
[16] Department of Physics, Applied Physics, and Astronomy, Rensselaer Polytechnic Institute, 110 Eighth Street, Troy, NY 12180-3590.
[17] Department of Astronomy and Astrophysics, 525 Davey Laboratory, Pennsylvania State University, University Park, PA 16802.
[18] Astrophysikalisches Institut Potsdam, An der Sternwarte 16, D-14482 Potsdam, Germany.
[19] National Astronomical Observatory, 2-21-1 Osawa, Mitaka, Tokyo 181-8588, Japan.
[20] See also http://www.astro.princeton.edu/PBOOK/welcome.htm.
[21] We refer to the measured magnitudes as u^*, g^*, r^*, i^*, and z^* because the absolute calibration of the SDSS photometric system is still uncertain at the ~ 0.05 mag level. The SDSS filters themselves are referred to as u', g', r', i', and z'. All magnitudes are given on the AB$_\nu$ system (Oke & Gunn 1983; for additional discussion regarding the SDSS photometric system, see Fukugita et al. 1996 and Fan 1999).

seeing. Astrometric positions are accurate to about 0".1 for sources brighter than 20.5 mag, and the morphological and color information from the images allows robust star-galaxy separation to ~21.5 mag.

The survey is being done with a dedicated, special-purpose 2.5 m telescope (Siegmund et al. 2000). It has a wide, well-corrected field (3°) and is equipped with a large mosaic CCD camera and a pair of fiber-fed spectrographs. The camera utilizes 30 large-area (2048 × 2048) CCDs (Gunn et al. 1998; Doi et al. 2000), which take the data in drift-scanning (time-delay and integrate) mode with a total integration time of 54.1 s. The imaging data are obtained using the data acquisition system at the Apache Point Observatory (Petravick et al. 1994; Annis et al. 2000) and recorded on digital linear tape. These tapes are shipped to Fermilab by express courier, and the data are automatically reduced through a set of software pipelines operating in a common computing environment (Kent et al. 2000). The photometric pipeline (Lupton et al. 2000) reduces the imaging data, measuring positions, magnitudes, and shape parameters for all detected objects. The photometric pipeline uses position calibration information from the astrometric pipeline (Pier et al. 2000) and photometric calibration data from the photometric telescope (Smith et al. 2000; Uomoto et al. 2000), reduced through the photometric telescope pipeline (Tucker et al. 2000). Final calibrations are applied by the final calibration pipeline, which allows refinements in the positional and photometric calibration to be applied as the survey progresses. The outputs, together with all the observing and processing information, are loaded into the operational database (Yanny et al. 2000b), which is the central repository of scientific and bookkeeping data used to run the survey.

About 40% of the sky in the northern survey will be surveyed twice (because of the scan overlaps), and all of the southern survey dozens of times (to search for variable objects and, by stacking the frames, to go deeper). Although two observations are normally insufficient to characterize a variable object, the multicolor nature of the photometric data helps enormously. Close to 1000 deg² of sky along the celestial equator have been observed during the SDSS commissioning phase (see, e.g., Fan et al. 1999). About 100 deg² of sky have been observed more than once; we use these data to search for variable objects. In this paper, we describe the detection and analysis of ~150 variable objects, probably RR Lyrae stars. Detecting RR Lyrae stars is important for Galactic structure studies because

They are believed to be an unbiased tracer of the low-metallicity halo population for kinematic studies (Hawkins 1984);

They are nearly standard candles ($\langle M_V \rangle = 0.7 \pm 0.1$; Layden et al. 1996), and thus it is straightforward to determine their distance; and

They are sufficiently bright to be detected at large distances (~100 kpc for $r' \sim 21$ mag) and are thus especially well suited for studies of the outer halo (Saha 1984). For a comprehensive review of RR Lyrae stars, we refer the reader to Smith (1995).

Wetterer & McGraw (1996) recently compiled data from several available deep searches for RR Lyrae stars in the outer Galactic halo. They pointed out that there are only nine RR Lyrae stars discovered at Galactocentric distances larger than 30 kpc, and only a few more have been found since then (see, e.g., Margon & Deutsch 1999 and references

therein). This paper presents a sample of candidate RR Lyrae stars with 81 stars estimated to be at such distances. The following section describes the selection procedure used in the search for candidate RR Lyrae stars and the resulting sample. We analyze the Galactic distribution of selected stars in § 3 and compare the sample with two other surveys of variable stars in § 4.

2. SELECTION PROCEDURE

We utilize imaging data from four runs (77, 745, 752, and 756) obtained during the SDSS commissioning phase. The data were obtained in six parallel scan lines,[22] each 13.5 wide, along the celestial equator ($-1°2687 <$ decl. $<$ 1°2676). The seeing in all runs was variable between 1″ and 2″ (FWHM), with the median value typically 1″.5. Runs 745 and 756, which are used as the main data set, were taken 1.9946 days apart on 1999 March 20 and 22. Their overlap extends from R.A. = 10^h42^m ($l = 248°6$, $b = 48°7$) to R.A. = 15^h46^m ($l = 7°3$, $b = 40°2$) and covers 97.5 deg² of sky (all coordinates are given as J2000.0).

As auxiliary control data sets, we use overlaps between runs 77 and 745 (33.7 deg²), 77 and 756 (20.5 deg²), and 752 and 756 (11.1 deg²). The right ascension ranges for these overlaps are summarized in Table 1. Run 77 was obtained on 1998 June 27 and provides a ~9 month baseline (266 and 268 days) when compared with runs 745 and 756. Run 752 was obtained on 1999 March 21 and provides a baseline of 0.9976 days when combined with run 756. The overlap between runs 752 and 756 perpendicular to the scan direction (i.e., declination overlap) is only 12.4% of the scan-line width (these are two six-column strips that are later interleaved to make a filled stripe of imaging data), while the overlaps between runs 77-745, 77-756, and 745-756 are 67.7%, 63.7%, and 95.9% of the scan-line width, respectively (scan-line width = 6 × 0°2253 = 1°3518).

RR Lyrae stars have the colors of A and F stars (Preston 1959; for SDSS colors, see Fukugita et al. 1996 and Krisciunas, Margon, & Szkody 1998; note also Fig. 2 below) and thus could be selected by appropriately constraining all four SDSS colors and then searching for variability. However, this would produce complicated selection effects because not all five bands have the same sensitivity. In order to avoid such effects, we follow a two-step procedure; the first step uses only data from the most sensitive, g' and r',

---

[22] See also http://www.astro.princeton.edu/PBOOK/strategy/strategy.htm.

TABLE 1

OVERLAPS BETWEEN SDSS COMMISSIONING RUNS

Runs	Min. R.A.[a]	Max. R.A.[b]	Area[c]	Δt[d]
745-756	10 42	15 46	97.5	1.9946
77-745	14 10	16 39	33.7	266.10
77-756	14 10	15 46	20.5	268.09
752-756	09 41	15 46	11.1	0.9976

NOTE.—Units of right ascension are hours and minutes.
[a] Starting right ascension for the overlap.
[b] Ending right ascension for the overlap.
[c] Total area in the overlap (deg²).
[d] Time elapsed between the two observations (in days).

bands, and only in the second step do we introduce color cuts based on data in all five bands. Throughout this work we use the "point-spread function" (PSF) magnitudes (measured by fitting a PSF model of a double Gaussian) as computed by the photometric pipeline (PHOTO, version v5_1; for details see Lupton et al. 2000).

Since RR Lyrae stars are bluer in $g^* - r^*$ than most other stars, we started our search by selecting the 90,569 unresolved and unsaturated sources with $-0.1 < g^* - r^* < 0.4$ from $\sim 930,000$ stars in the overlap of runs 745 and 756 and then required that candidate variable sources satisfy the following conditions:

1. The difference between the magnitudes in the two runs in both g' and r' bands is at least 0.15.
2. The difference between the magnitudes in the two runs in both g' and r' bands is at least 5 σ. Here the errors are taken as estimated by the photometric pipeline and do not include systematic calibration errors. However, because of the above requirement (variability of at least 0.15 mag), this condition becomes relevant only at the faint end, where the errors are dominated by photon statistics (see Fig. 1 below).
3. Candidates are brighter in r^* when they are bluer in $g^* - r^*$ (since RR Lyrae stars are pulsating variable stars). This is equivalent to the condition that the difference between the magnitudes in g' is larger than the difference between the magnitudes in r'. This condition is implemented without accounting for photometric errors.

These selection criteria yield 186 candidates. In Figure 1a, the large dots show the observed change in the r^* magnitude for the selected candidates plotted as a function of the mean r^* magnitude. The small dots mark the remaining 90,569 sources with $-0.1 < g^* - r^* < 0.4$. The two dashed lines show the boundary of the observational cutoff (the combination of items 1 and 2 above). The mean errors (for the magnitude difference) are about 0.03 mag up to 20 mag, increasing to about 0.07 mag at 21 mag, and to 0.2 mag at 22 mag; the observed error distribution is in good agreement with the errors quoted by the photometric pipeline.

There are 21 stars ($\sim 10\%$) rejected by the third condition $|g_2^* - g_1^*| > |r_2^* - r_1^*|$, where subscripts 1 and 2 mark data from each epoch. This condition is shown by the diagonal dashed line in Figure 1b, where, for clarity, only stars with mean $r^* < 20$ are plotted (using the same symbols as in Fig. 1a). Note that Figures 1a and 1b show two projections of the three-dimensional selection volume spanned by $g_2^* - g_1^*$, $r_2^* - r_1^*$, and the mean r^* magnitude. The rejected candidates are probably W Ursae Majoris stars but may also be RR Lyrae stars scattered across the selection boundary by photometric errors. The former probably dominate in the rejected subsample because more than 80% are brighter than $r^* = 20$ and thus have very small photometric errors. The diagonal solid line in Figure 1b shows a best-fit relation $|g_2^* - g_1^*| = 1.4 |r_2^* - r_1^*|$. Similar analysis based on data from other bands yields $|u_2^* - u_1^*| = 1.0 |g_2^* - g_1^*|$, $|r_2^* - r_1^*| = 1.2 |i_2^* - i_1^*|$, and
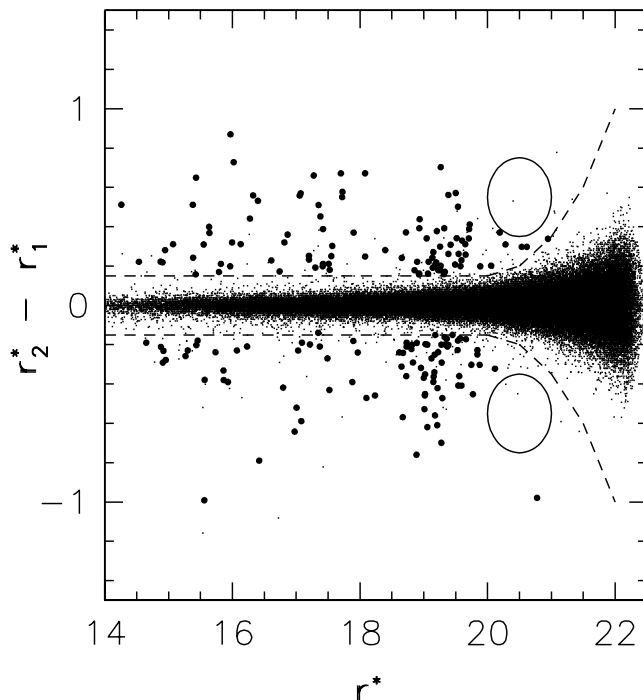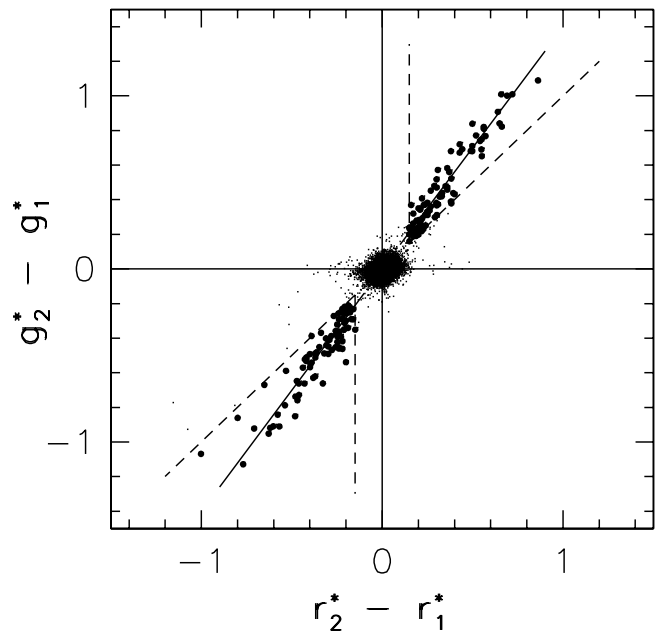

FIG. 1a

FIG. 1b

FIG. 1.—(a) Observed change of r^* magnitude plotted against the mean r^* magnitude for 90,569 unresolved sources with $-0.1 < g^* - r^* < 0.4$, marked as small dots. Large dots mark 186 sources that satisfy $|\Delta g^*| > 0.15$ mag, $|\Delta r^*| > 0.15$ mag, at least 5 σ variability in both g' and r' bands, and which are brighter in r^* when they are bluer in $g^* - r^*$. The two dashed lines show the boundary of the variability cutoff. The lack of faint objects with large amplitudes in the regions outlined by the two ellipses indicates that we are detecting the faint end of the RR Lyrae magnitude distribution and, hence, the limit of their distance distribution. Note that the absence of such sources is not due to our selection criteria, since sources in those two regions are already absent in the starting sample (*dots*). (b) Observed change of g^* magnitude plotted against the observed change of r^* magnitude for sources from (a) that satisfy $r^* < 20$. The meaning of the symbols is the same as in (a). Vertical dashed lines show the selection conditions $|\Delta g^*| > 0.15$ mag, $|\Delta r^*| > 0.15$ mag, and the diagonal dashed line shows the condition $|\Delta g^*| > |\Delta r^*|$ (or, equivalently, brighter in r^* when bluer in $g^* - r^*$). The diagonal solid line shows a best-fit relation $|g_2^* - g_1^*| = 1.4 |r_2^* - r_1^*|$. [*See the electronic edition of the Journal for color versions of Figs. 1–9.*]
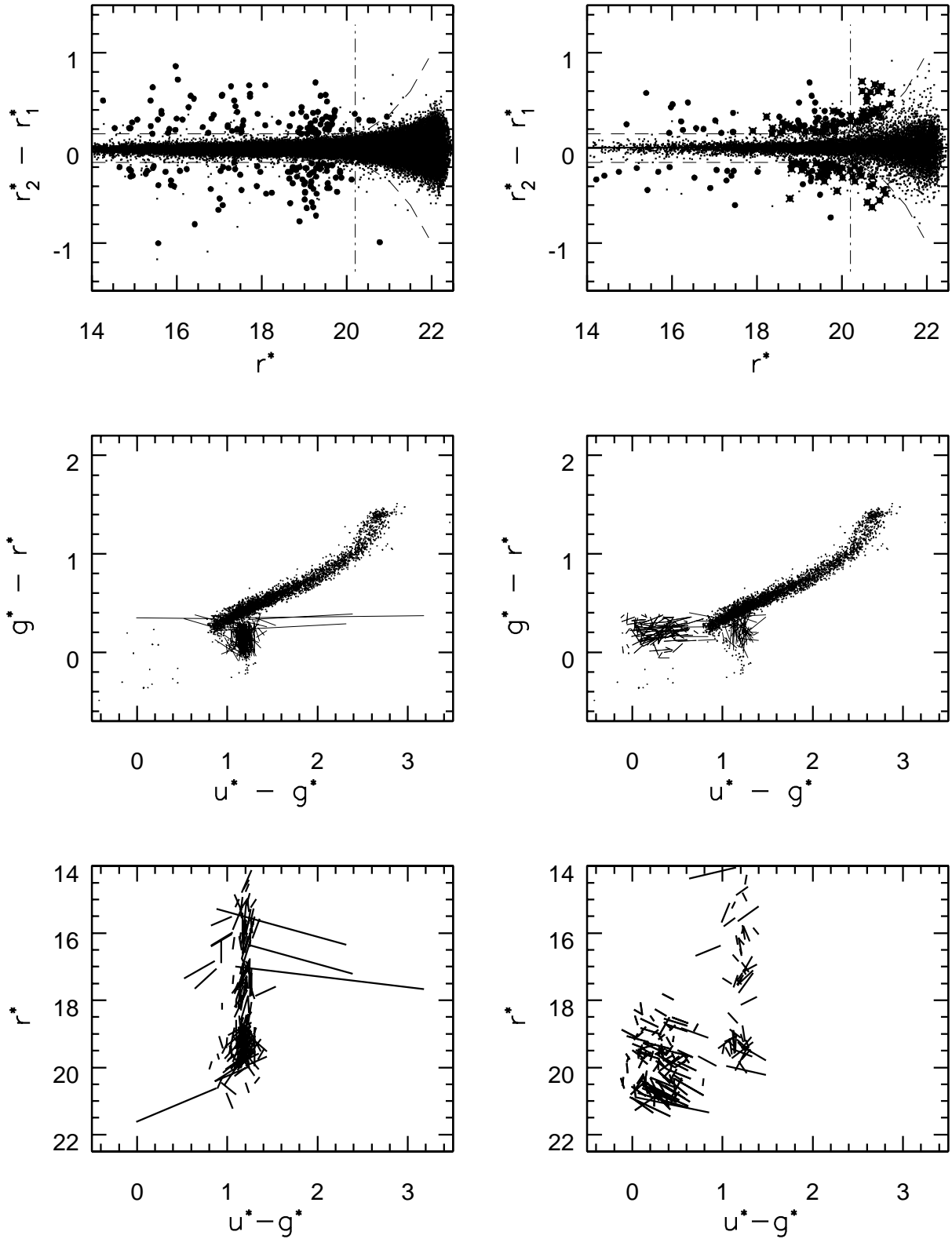
FIG. 2.—Comparison of two searches for RR Lyrae stars: the left column is for 100 deg² of sky observed 2 days apart, and the right column is for 35 deg² of sky observed 9 months apart. The top two panels are analogous to Fig. 1a (the distribution of nonvariable objects in the left panel appears to be somewhat wider because it includes ∼3 times more sources). Vertical lines at $r^* = 20.2$ are added to guide the eye and mark the faint end of the RR Lyrae star magnitude distribution. Sources with $u^* - g^* < 0.8$ are marked by crosses and represent variable QSOs rather than RR Lyrae stars. Their color difference can be seen in the two middle panels, which show $u^* - g^*$ vs. $g^* - r^*$ diagrams. In these diagrams, variable sources are marked by lines that connect photometric measurements at the two epochs. Dots represent a subsample of 5000 nonvariable objects and clearly outline the stellar locus. Note that there are no variable sources with $u^* - g^* < 0.8$ in the left panel since QSOs do not vary sufficiently on a 2 day timescale. The lower two panels display r^* vs. $g^* - r^*$ color-magnitude diagrams and show that we detect no RR Lyrae stars fainter than $r^* \sim 20$ even though variable QSOs, which are selected by identical criteria, are detected to $r^* > 21$.

$|i_2^* - r_1^*| = 1.1 |z_2^* - i_1^*|$, where the uncertainty of best-fit coefficients is $\lesssim 0.05$.

A striking feature in Figure 1a is the lack of faint objects with large variability amplitudes in the regions outlined by the two ellipses. The magnitude distribution of the RR Lyrae candidates turns off rather sharply at $r^* \sim 20$, even though nonvariable objects are detected 2.5 mag fainter, and the errors are sufficiently small that variable sources with similar amplitudes could be detected to at least $r^* \sim 21$ (see below). This indicates that we are detecting the faint end of the RR Lyrae magnitude distribution and, hence, the limit of their distance distribution. The absence of faint variable sources appears not to be due to our selection criteria, since sources in those two regions are already practically absent in the starting sample (Fig. 1a, *small dots*). To repeat, the starting sample was selected from the full data set by simply extracting unresolved[23] sources in the appropriate $g^* - r^*$ color range.

Additional support for the reality of this cutoff comes from the analysis of the overlap between runs 77 and 745. These runs were obtained 9 months apart, which is a sufficiently long baseline to detect quasar (QSO) variability. Although low-redshift QSOs ($z < 2$) have $g^* - r^*$ colors similar to RR Lyrae stars, they are easily distinguished by their bluer $u^* - g^*$ colors (Fan 1999). Since variable QSOs should not have a faint-magnitude cutoff, they can be used to test whether the data allow the detection of variable sources fainter than $r^* \sim 20$.

We searched for variable objects in the overlap of runs 77 and 745 (~ 35 deg^2) using the same criteria outlined above. This new search is summarized in the right panels in Figure 2 and compared with the results from the first search shown in the panels on the left. The top two panels are analogous to Figure 1a (indeed, the top left panel is the same). Vertical lines at $r^* = 20.2$ are added to guide the eye, and to mark the apparent faint end of the RR Lyrae magnitude distribution detected in runs 745-756. QSOs are selected by requiring $u^* - g^* < 0.8$ and are marked by crosses.[24] The color difference between QSOs and RR Lyrae stars can be easily seen in the $g^* - r^*$ versus $u^* - g^*$ color-color diagrams shown in the two middle panels.[25] In these diagrams, variable sources are marked by lines that connect photometric measurements at the two epochs, and dots represent a subsample of 5000 nonvariable unresolved objects that outline the stellar locus and the position of low-z QSOs ($u^* - g^* < 0.8$). Note that there are no variable sources with $u^* - g^* < 0.8$ in the left panel, since QSOs do not vary much on a 2 day timescale. The bottom two panels display r^* versus $g^* - r^*$ color-magnitude diagrams and show that we detect no RR Lyrae stars fainter than $r^* \sim 20$ even though variable QSOs, which are selected by identical criteria, and without using the u'-band data, are detected to $r^* > 21$.

The described search procedure deliberately used only g'- and r'-band data in the first step in order to simplify selec-
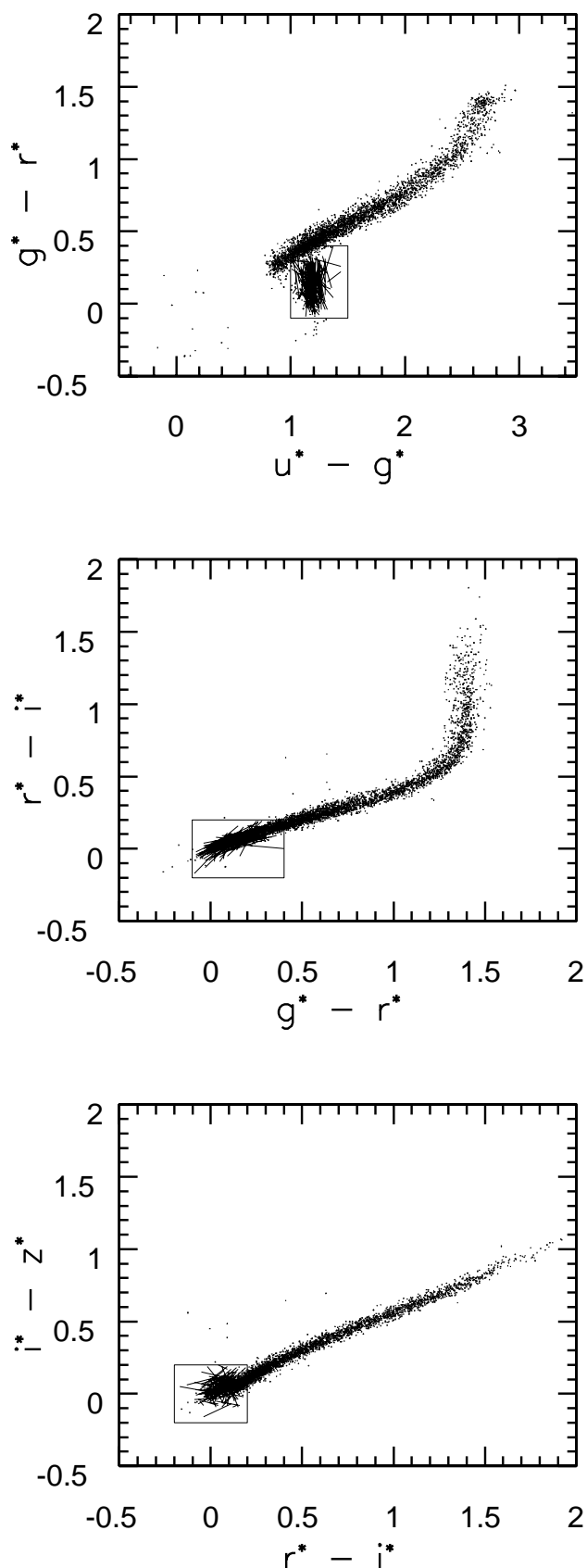
FIG. 3.—Color-color diagrams displaying the final RR Lyrae sample of 148 stars marked by lines that connect photometric measurements at the two epochs. Dots represent a subsample of nonvariable unresolved objects and outline the stellar locus. The final RR Lyrae sample was selected from the 186 candidates shown in Fig. 1a by imposing color cuts, displayed as boxes.

[23] Ignoring the requirement that candidates must be unresolved has practically no effect on the resulting sample. Thus, possible star-galaxy misclassification cannot be invoked as an explanation for the observed cutoff.

[24] Detailed analysis of the variable QSO sample is outside the scope of this work and will be presented in a separate publication.

[25] In all color-color diagrams, blue is toward the lower left corner and red is toward the upper right corner.

tion effects, and thus to show that the faint-magnitude limit of selected candidate RR Lyrae stars is real. For subsequent analysis, however, we further constrain the sample to sources with colors appropriate for RR Lyrae stars ($1.0 < u^* - g^* < 1.5, -0.1 < g^* - r^* < 0.4, -0.2 < r^* - i^* < 0.2, -0.2 < i^* - z^* < 0.2$). These limits are shown as boxes in the color-color diagrams displayed in Figure 3 and result in the final sample of 148 stars. Thus, 80% of the sources in the initial sample of 186 stars pass these tight additional criteria, showing that candidate RR Lyrae stars can be quite efficiently selected with only two-epoch, two-band (g' and r') data with a sufficiently short baseline to avoid contamination by variable QSOs. About two-thirds of the 38 rejected sources narrowly fail one or two of the imposed color limits, and the remaining third usually fail by more than 0.5 mag in a single color, most often in $u^* - g^*$ and $i^* - z^*$. While the former may be RR Lyrae stars, the latter are more likely to belong to different types of variable binary stars. The inclusion of the rejected sources in the subsequent analysis does not significantly change the resulting volume density of the selected candidates. However, it affects the estimated statistical significance of the observed cutoff in the candidates' magnitude distribution at $r^* \sim 20$ (§ 4.1).

3. ANALYSIS OF THE CANDIDATE RR LYRAE STARS

The colors and variability properties of 148 stars in our final sample are consistent with their being RR Lyrae stars (Krisciunas et al. 1998). In particular, our observations were obtained ~2 days apart and thus are sensitive to the variability timescales characteristic for these stars (0.3–0.8 days; Saha 1984), while insensitive to objects varying on longer timescales (QSOs, long-period variables, etc.). In addition, the brightness variations are consistent with RR Lyrae amplitudes (0.7–1.5 mag peak to peak; Saha 1984), and the candidates are bluer at the brighter epoch. While contamination by variable stars of similar properties (e.g., dwarf Cepheids or SX Phoenicis stars) cannot be excluded without detailed light curves, spectroscopic data, or both, the expected level of contamination is probably not larger than 10% (Harris 1993; Guhathakurta et al. 1994; see also
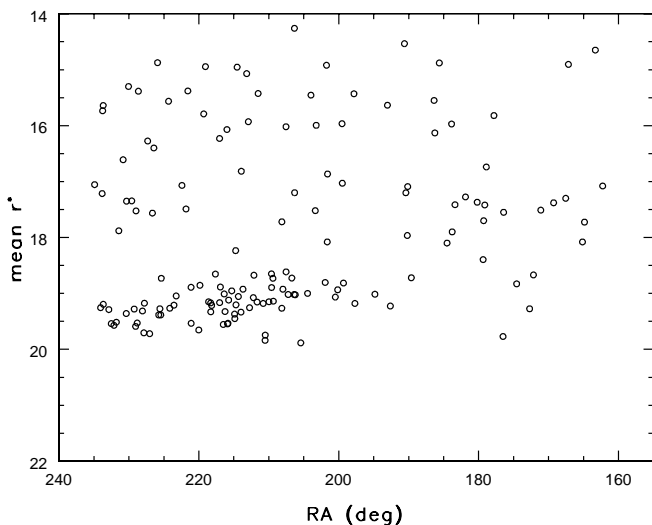
§ 4.3). We will assume in the rest of this work that all sources in the final sample are RR Lyrae stars.

The selected candidate RR Lyrae stars are not smoothly distributed in magnitude, as can be seen in Figures 1 and 2. This clumpiness is also seen in their angular distribution. Figure 4 shows the distribution of candidate RR Lyrae stars in the mean r^* versus right ascension diagram. There is an obvious concentration of ~70 sources with $r^* \sim 19$–19.5 and $205° < $ R.A. $ < 230°$. This feature is present in all six data columns (separated in declination), and the column-to-column scatter of counts in these right ascension and r^* ranges is consistent with Poisson statistics.

To test this feature further, we analyze additional two-epoch data from several different run combinations. As before, the detection of variable QSOs in the overlap of runs 77 and 745 allows a powerful test because variable QSOs should not display any spatial structure on such a large angular scale ($\gtrsim 10°$). The distribution of variable objects detected in these two runs in the mean r^* versus right ascension diagram is shown in Figure 5 (note the different right ascension limits here from those in Fig. 4). Sources with $u^* - g^* > 0.8$, candidate RR Lyrae stars, are marked by circles and the sources with $u^* - g^* < 0.8$, presumably variable QSOs, are marked by squares. While QSOs are homogeneously distributed as expected, the distribution of candidate RR Lyrae stars is markedly different even though both samples were selected by identical criteria. At the same time, the distribution of candidate RR Lyrae stars, most notably the concentration of sources with $r^* \sim 19$–19.5 at $215° < $ R.A. $ < 230°$, is in agreement with the results obtained from the overlap of runs 745 and 756 and shown in Figure 4. An overdensity of candidate RR Lyrae stars in the same magnitude–right ascension region is also detected in overlaps from runs 77-756 and 752-756.

A stellar overdensity analogous to that of candidate RR Lyrae stars in the region $205° < $ R.A. $ < 230°$ can also be seen in the distribution of nonvariable sources with similar colors. Figure 6 displays the mean r^* versus right ascension

Fig. 4.—Distribution of candidate RR Lyrae stars in the mean r^* vs. right ascension diagram. Note the concentration of sources with $r^* \sim 19$–19.5 and $205° < $ R.A. $ < 230°$.
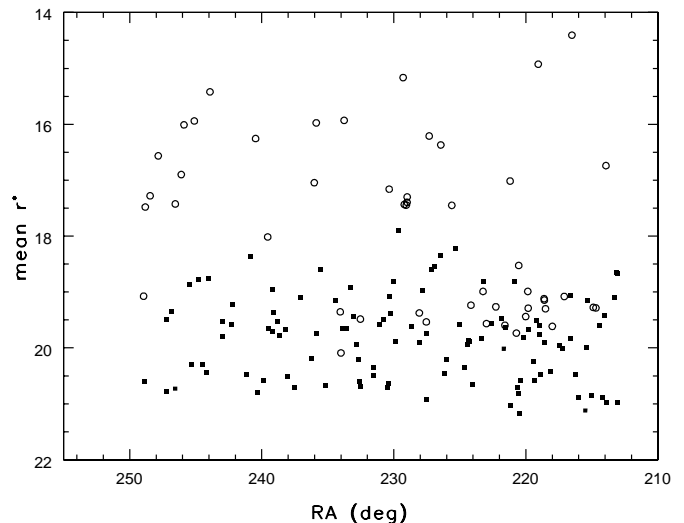
Fig. 5.—Distribution of candidate RR Lyrae stars detected in two runs obtained 9 months apart in the mean r^* vs. right ascension diagram. Sources with $u^* - g^* > 0.8$, presumably RR Lyrae stars, are marked by circles, and the sources with $u^* - g^* < 0.8$, presumably QSOs, are marked by squares. Note that the distribution of RR Lyrae stars, most notably the concentration of sources with $r^* \sim 19$–19.5 at $215° < $ R.A. $ < 230°$, is markedly different from the homogeneous distribution of QSOs, even though both are selected by identical criteria.

FIG. 6.—Distribution of 587 stars from the overlap of runs 745 and 756 satisfying $1.1 < u^* - g^* < 1.5$ and $-0.1 < g^* - r^* < 0.3$ in the mean r^* vs. right ascension diagram. Note the concentration of sources with $r^* \sim 19$–19.5 and $205° <$ R.A. $< 230°$, the same magnitude–right ascension range as for the concentration of candidate RR Lyrae stars displayed in Fig. 4.

FIG. 7.—An r^* vs. $g^* - r^*$ color-magnitude diagram for ~ 2000 stars observed in SDSS commissioning run 756 inside a circle with 5′ radius and centered on the position of the core of globular cluster Palomar 5. Five stars selected as candidate RR Lyrae stars are marked by lines that connect measurements at different epochs; all fall in the appropriate blue horizontal-branch region for Palomar 5 ($g^* \sim 17.5$).

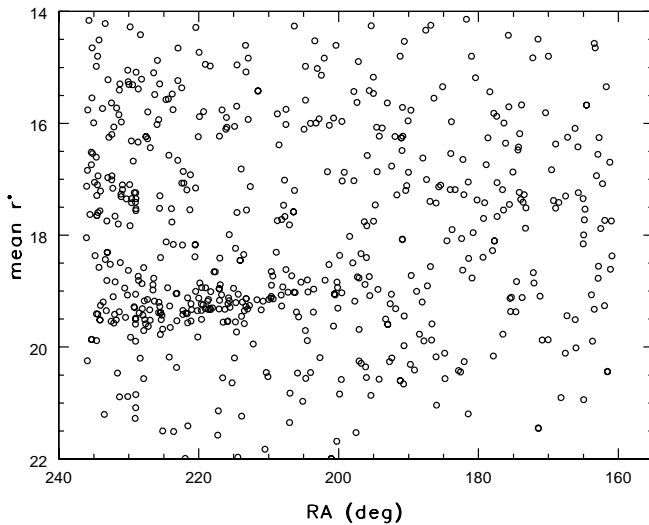diagram for 587 stars from the overlap of runs 745 and 756 satisfying $1.1 < u^* - g^* < 1.5$ and $-0.1 < g^* - r^* < 0.3$. The concentration of sources with $r^* \sim 19$–19.5 and $205° <$ R.A. $< 230°$, the same magnitude–right ascension range as for the overdensity of candidate RR Lyrae stars displayed in Figure 4, is easily discernible and provides additional evidence for the clump. We used somewhat tighter color criteria than in the search for candidate RR Lyrae stars, in order to decrease contamination by F stars from the blue tip of the stellar locus (cf. Fig. 2). However, this contamination cannot be entirely removed by using only color cuts, and sources with $r^* > 20$ displayed in Figure 6 are probably main-sequence or blue straggler stars (i.e., with smaller luminosities than RR Lyrae stars, and thus intrinsically fainter). Yanny et al. (2000a) also detect this clump and another smaller clump in the southern Galactic hemisphere in SDSS commissioning data by analyzing the distribution of stars with similar colors ($0.8 < u^* - g^* < 1.5$ and $-0.3 < g^* - r^* < 0.0$).

A group of sources at R.A. $\sim 230°$ and $r^* \sim 17.5$ can be seen in both Figures 5 and 6. These sources belong to the globular cluster Palomar 5 (Rosino 1951; Abell 1955; Wilson 1955) and represent its blue horizontal-branch stars. Figure 7 displays an r^* versus $g^* - r^*$ color-magnitude diagram for ~ 2000 stars observed in run 756 inside a circle with 5′ radius and centered on the position of the Palomar 5 core (R.A. = $15^{\text{h}}16^{\text{m}}5^{\text{s}}.3$, decl. = $-0°6'41''$, J2000.0). Five stars selected here as candidate RR Lyrae stars (from the overlaps 745-756, 77-745, and 77-756) are marked by lines that connect measurements at different epochs, and all fall in the appropriate blue horizontal-branch region for Palomar 5 ($g^* \sim 17.5$; Smith et al. 1986). This further reinforces the assumption that our selection criteria reliably select RR Lyrae stars.

3.1. Galactic Distribution of Candidate RR Lyrae Stars

The observed magnitudes of candidate RR Lyrae stars can be used to infer their distances and, consequently, their
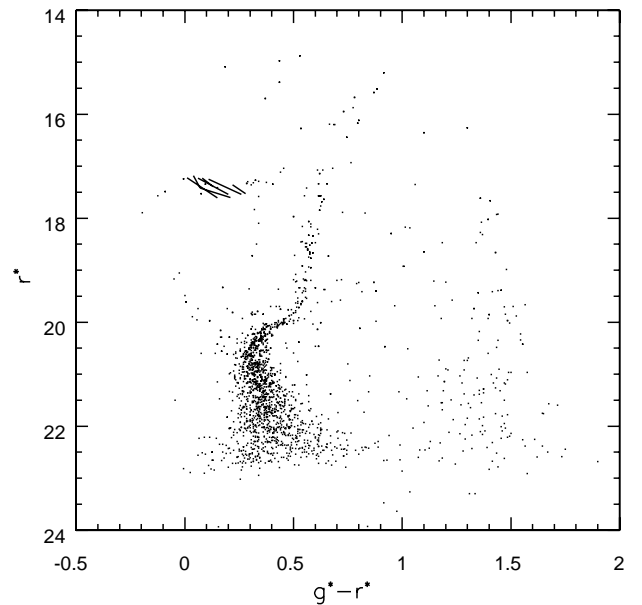
Galactic distribution. We calculate distances to stars in the final sample by assuming constant luminosity of $M_V = 0.7$ mag (Layden et al. 1996) and transformation $M_V = M_{r_*} + 0.44(g^* - r^*) - 0.02$ (Krisciunas et al. 1998), which typically results in $M_V - M_{r_*} \sim 0.05$ mag. For the apparent brightness estimate, we use the mean r^* magnitude corrected for the interstellar extinction, and for a 0.1 mag bias due to asymmetric RR Lyrae light curves (see Appendix). Typical values of the interstellar extinction, as determined from the maps given by Schlegel, Finkbeiner, & Davis (1998), are $A_{r_*} = 0.05$–0.15 ($A_{g_*} = 1.38 A_{r_*}$).

Figure 8 shows the Galactic distribution of candidate RR Lyrae stars, displayed as small circles (the large circle marks the Sun's position at $X = -8$ kpc, $Y = 0$, $Z = 0$). The dashed lines show the volume within which our data can detect RR Lyrae stars: a very thin wedge with an opening angle of $80°$ and distances ranging from 5 kpc (saturation limit, $r^* \sim 14$) to 90 kpc (faint limit, $r^* \sim 21$). The dotted lines show the intersection of this wedge with a Galactocentric sphere of radius 30 kpc ($r^* \sim 18$–18.5).

The clump of candidate RR Lyrae stars centered on $X = 20$ kpc, $Y = 10$ kpc, $Z = 40$ kpc corresponds to the concentration of sources with $r^* \sim 19$–19.5 and $205° <$ R.A. $< 230°$ visible in Figure 4. The clump center is in a similar direction ($l = 340°$, $b = 60°$) to the center of the Sagittarius dwarf spheroidal galaxy at $l = 5°.6$, $b = -14°.0$. The Sagittarius dwarf spheroidal is the closest known Galactic satellite, with a Galactocentric distance of 16 ± 2 kpc (Ibata et al. 1997). In the coordinate system displayed in Figure 8 it is situated at $X = 15$ kpc, $Y = -2$ kpc, $Z = -6$ kpc, and it is marked by a triangle in the middle panel. The distance between its center and the clump is ~ 50 kpc. This is significantly larger than the extent of either structure (~ 10 kpc) and probably implies that they are not physically associated. It is interesting, however, that the Galactic orbit
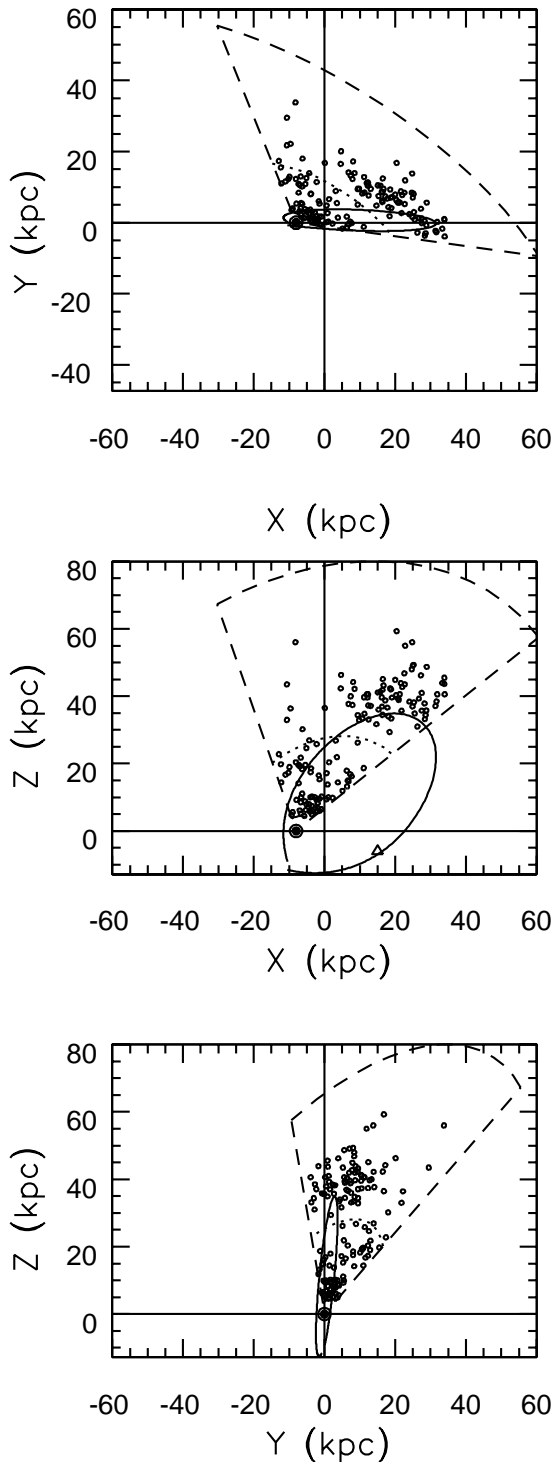
of the Sgr dwarf spheroidal, as calculated by both Ibata et al. and Johnston et al. (1999a), crosses the clump of candidate RR Lyrae stars. We display this orbit, taken from Johnston et al. (1999a), by a solid line in Figure 8 (the direction of the Sgr dwarf's motion is toward the clump). Such close proximity between the calculated orbit and the clump of candidate RR Lyrae stars may perhaps be evidence of presumed debris caused by tidal disruption of the Sgr dwarf spheroidal (Johnston et al. 1999a, 1999b; Ibata et al. 2000) in the Galactic potential. Additional observations of the surrounding area, and the radial velocity measurements for the clump stars, are required to further explore this hypothesis.

From the Galactic distribution of candidate RR Lyrae stars presented in Figure 8, we calculate their volume density as a function of Galactocentric radius and display it as data points with 1σ error bars in Figure 9. The uncertainties are determined from Poisson statistics in the vertical direction and from the bin width in the horizontal direction. Since two-epoch data cannot detect all RR Lyrae stars, the overall normalization of the volume density includes unknown selection efficiency. We estimate that the selection efficiency is 56%, from a Monte Carlo study based on a set of model light curves with realistic amplitude and period distributions (for details see Appendix). This estimate agrees well with two independent determinations described in § 4.3 below.

Wetterer & McGraw (1996) used a large compilation of available RR Lyrae searches to find that their distribution follows an R^{-3} power law, where R is the Galactocentric radius. This is plotted as the solid line in Figure 9; the thin

Fig. 8.—Galactic distribution of selected candidate RR Lyrae stars (*open circles*). The Sun (*large circle*) is at $(X = -8$ kpc, 0, 0). The dashed lines show the volume within which our data can detect RR Lyrae stars: a very thin wedge with an opening angle of 80° and distances ranging from 5 kpc (saturation limit) to 90 kpc (faint limit). Dotted lines are added to guide the eye and show the intersection of this wedge with a Galactocentric sphere of radius 30 kpc ($r^* \sim 18$–18.5). Note the group of candidate RR Lyrae stars at $X = 20$ kpc, $Y = 10$ kpc, $Z = 40$ kpc, corresponding to the concentration of sources with $r^* \sim 19 - 19.5$ and $205° <$ R.A. $< 230°$ visible in Fig. 4. The solid line displays the orbit of the Sgr dwarf spheroidal (situated at $X = 15$ kpc, $Y = -2$ kpc, $Z = -6$ kpc and marked by a triangle in the middle panel) as calculated by Johnston et al. (1999a).

Fig. 9.—Comparison between the volume density for RR Lyrae stars obtained from our data (*dots with error bars*) and the R^{-3} power law determined by Wetterer & McGraw (1996, solid line with the 1σ uncertainty shown by thin dot-dashed lines). We find that the volume density follows a shallower power law with a best-fit power index of 2.7 ± 0.2 (*thick dot-dashed line*) for $R < 50$ kpc and turns off sharply as a rather steep $R^{-11.2}$ power law for $R > 60$ kpc (*dashed line*). Data for $R < 35$ kpc are consistent with the R^{-3} distribution.

dot-dashed lines represent their 1 σ normalization uncertainty (factor of ~ 2). We find two noteworthy deviations from this power law. First, our analysis indicates that the RR Lyrae volume density may follow a shallower power law with a best-fit index of 2.7 ± 0.2. Second, the absence of RR Lyrae stars with $r^* > 20$ implies a rather sharp halo edge at $R_{halo} = 50$–60 kpc. Figure 9 shows two power-law fits: the thick dot-dashed line is the $R^{-2.7}$ power law determined for data with $R < 60$ kpc, and the dashed line is the steep $R^{-11.2}$ power law determined for data with $R > 50$ kpc. The latter power law is shown only for illustration and should not be taken literally (there are only two data points at $R > 50$ kpc). Note that this sample is neither large enough nor sufficiently extended over the sky to constrain the halo flattening (see, e.g., Hartwick 2000).

These results imply that there are 2–3 times more RR Lyrae stars at $R \sim R_{halo}$ than predicted by the Wetterer & McGraw power law. However, it is obvious that a shallower power law is obtained mainly because of the large number of candidates in the "45 kpc" clump. When they are excluded by constraining the sample to radii less than 35 kpc, the best-fit power-law fit becomes $R^{-3.1 \pm 0.2}$, in agreement with the Wetterer & McGraw result, including the normalization at the bright end. The same result is obtained when the sample is constrained to $160° <$ R.A. $< 200°$ (see Fig. 4), and in this case the fit is satisfactory all the way to $R \sim 50$ kpc. This may indicate that the halo contains clumpy overdensities inhomogeneously distributed within an underlying smooth R^{-3} density distribution.

4. DISCUSSION

4.1. Statistical Significance of the Observed Cutoff at $R \sim 50$ kpc

The statistical significance of the observed lack of candidate RR Lyrae stars with $r^* > 20$ can be determined from the expected number of candidates with such magnitudes. However, it is difficult to estimate this number with certainty because of the observed clumpy spatial distribution of selected candidates, and because of only weakly constrained selection effects at the faint end. We estimate the expected number of candidates with $r^* > 20$ by extrapolating the R^{-3} power-law density to infinity (this power law implies a flat magnitude distribution for sources with uniform luminosity).

A Monte Carlo study of the selection effects, described in the Appendix, finds that the selection efficiency starts to fall off slowly for $r^* > 19$, reduces to about 50% at $r^* \sim 20$, and drops to zero for $r^* \sim 21.5$. Confirmation of this falloff comes from analyzing the variable QSO sample. Assuming that the fraction of variable QSOs does not depend on their magnitude (we find this fraction to be $\sim 15\%$), the efficiency determined from simulations is in agreement with that implied by the observed numbers of variable QSOs (which, however, may have very different light curves). We adopt 25% as the mean efficiency in the $20 < r^* < 21.5$ magnitude range. In order to avoid the effects of the clumpy spatial distribution, we determine the expected density of candidates by considering only those satisfying $160° <$ R.A. $< 200°$ and $15 < r^* < 19$ (cf. Fig. 4). We estimate a density of 18 mag^{-1}, normalized to the entire right ascension range. With the adopted efficiency, we find that the expected number of candidate RR Lyrae stars with $r^* > 20$

is seven, while we have selected none. The Poisson probability for this outcome is $\sim 10^{-3}$.

A more conservative approach may be taken by considering all 186 candidates from the first selection step (i.e., before the color cuts described in § 2 were imposed to yield the final sample of 148 sources). As a result of a larger number of candidates, the expected number of sources with $r^* > 20$ is increased to nine. As can be seen in Figures 1a and 2, there are four sources that barely missed the cuts and could perhaps be RR Lyrae stars. The Poisson probability that four or fewer sources are observed, given the expectation value of nine, is ~ 0.02. As is evident, this approach significantly reduces the implied statistical significance of the observed cutoff at $r^* \sim 20$.

We conclude that the significance of the observed cutoff is at the level of 2–3 σ (in terms of equivalent Gaussian probability). The best way to improve this estimate is to obtain follow-up observations of the rejected sources to establish whether they are RR Lyrae stars, and of course to analyze data for a significantly larger sky area.

4.2. Comparison with FASTT and LONEOS Data

The final sample of candidate RR Lyrae stars presented here is based on commissioning data taken at only two epochs. In order to estimate the level of spurious variability detections, we have cross-referenced our list with the list of variable objects found from the FASTT (Flagstaff Astrometric Scanning Transit Telescope) data (Henden & Stone 1998) and with the LONEOS (Lowell Observatory Near-Earth Object Search) database.[26] The LONEOS data fully

---

[26] The LONEOS home page is http://asteroid.lowell.edu/asteroid/loneos/loneos_disc.html.
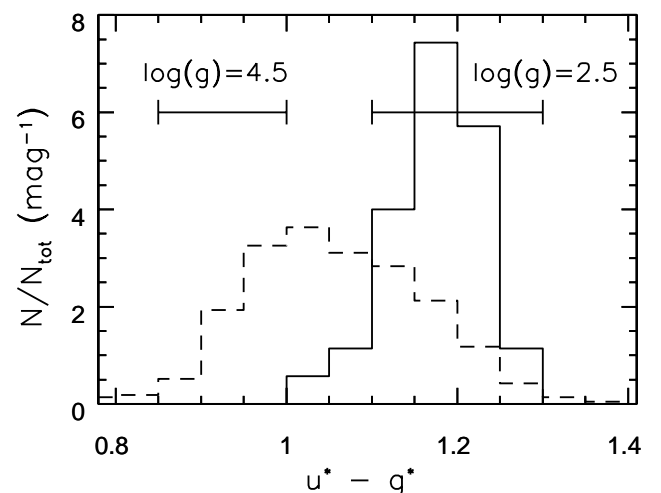
FIG. 10.—The $u^* - g^*$ color distribution for stars selected by $0.0 < g^* - r^* < 0.1$ (cf. Fig. 2) from the 90,569 stars shown in Fig. 1a (dashed line) and for stars selected by the same criterion from the resulting sample of candidate RR Lyrae stars (solid line). Note that the $u^* - g^*$ color of candidate RR Lyrae stars is on average redder for ~ 0.2 mag than the $u^* - g^*$ color of nonvariable stars within the same narrow range of $g^* - r^*$ color. Theoretical expectations taken from Lenz et al. (1998) are shown as horizontal lines. For main-sequence stars, the expected $u^* - g^*$ range is 0.85–1.0 (marked as $\log g = 4.5$), and for horizontal-branch stars the expected $u^* - g^*$ range is 1.1–1.3 (marked as $\log g = 2.5$). The intrinsic spread of the $u^* - g^*$ color for a given gravity is due to varying metallicity, and the plotted values correspond to the range $-2.0 < [M/H] < 0$.

cover the overlap of runs 745 and 756, while the overlap with the FASTT fields is only partial (~ 40 deg^2). Both data sets can detect variable stars brighter than $r^* \sim 17$.

Henden & Stone (1998) require that a candidate variable star show night-to-night scatter (typically eight to 12 epochs) larger than 3 times the expected error in the magnitude. Based on a random sampling of a set of model light curves with realistic amplitude and period distributions (see Appendix), we determine that the mean rms scatter for RR Lyrae stars is ~ 0.3 mag. The photometric accuracy of FASTT data (see Fig. 1 in Henden & Stone 1998) implies that the detection efficiency for RR Lyrae stars in FASTT data should drop sharply for $r^* > 17$ mag. The list of selected candidate RR Lyrae stars includes 16 sources that are sufficiently bright and in the FASTT fields. We find that 14 of them are indeed in the Henden & Stone list as published, and one was detected later from additional observations (A. Henden 1999, private communication). This implies a reliability of our selection procedure of 94%. The remaining source, with a mean $r^* = 14.9$ (SDSSp J110838.26−000514.3; see Table 2 below), is definitely variable in SDSS data, with amplitudes exceeding 0.15 mag in all five bands (0.34 mag in g^*). To estimate the efficiency of our two-epoch selection procedure, we matched all sources with appropriate colors (cf. § 2) detected in the SDSS data (8786 sources) to the Henden & Stone list and found 33 matches (note that here no magnitude limit is imposed). As we recovered 17 of them as candidate RR Lyrae stars, this implies an efficiency of 52% ± 15%, assuming that all Henden & Stone variable sources with appropriate SDSS colors are RR Lyrae stars.

The sensitivity of the LONEOS data for variability detection drops sharply for $r^* > 17$ mag, and 33 stars in our sample are brighter than this limit. For two of these stars, no LONEOS data are available (both stars are too close to much brighter objects). Of the remaining 31 stars, the LONEOS data clearly indicate variability for 29 (94%) and are inconclusive for the other two. Unfortunately, because of their coarse sampling in time, neither the LONEOS data nor the FASTT data can be used to produce light curves that could definitively identify the variable objects as RR Lyrae stars.

4.3. Contamination by Other Variable Stars

While the SDSS multicolor photometry indicates that all candidates discussed here have colors appropriate for RR Lyrae stars, there exist other types of variable stars with similar colors. For example, W Ursae Majoris stars can have F-type spectra, but they should be efficiently screened out by the selection requirement that candidates must be brighter in r^* when they are bluer in $g^* - r^*$.

The most significant contaminants are probably δ Scuti stars, another pulsating variable type with approximately the same color range as the RR Lyrae stars, periods of 1–3 hr, and magnitudes about 0.5 mag fainter than RR Lyrae stars (Hoffmeister, Richter, & Wenzel 1985). For example, the Tycho photometric survey finds that for $m_B < 11$ mag, the numbers of RR Lyrae stars and δ Scuti stars are comparable. However, the Population I δ Scuti stars should start to run out at a distance of ~ 2 kpc from the Galactic plane, or equivalently at $r^* < 13$ mag for $b > 30°$. On the other hand, the Population II δ Scuti stars, also known as SX Phoenicis stars, contribute only 10% to the δ Scuti population (G. Burks 1999, private communication). Thus, the

likely contamination of our sample should not be more than 10%, which would not qualitatively change our results. We note that this fraction may be somewhat larger if the number of SX Phoenicis stars decreases more slowly with Galactocentric radius than does the number of RR Lyrae stars. In the following section, we discuss multiepoch photometric observations for seven SDSS-selected candidate RR Lyrae stars and show that all observed light curves have shapes and periods typical for RR Lyrae stars. This result is consistent with the above estimate for the contamination fraction of $\lesssim 10\%$.

Another independent piece of evidence that our sample is dominated by the low-gravity RR Lyrae stars is that the $u^* - g^*$ colors for the selected candidates are redder than those of the parent population. It has long been known that Balmer jumps are larger for horizontal-branch stars than for main-sequence stars (e.g., Oke, Giver, & Searle 1962; Pier 1983). The resulting $u^* - g^*$ colors for horizontal-branch stars are redder than for main-sequence stars, given the same $g^* - r^*$ color (Lenz et al. 1998). Figure 10 shows the $u^* - g^*$ color distribution for stars selected by $0.0 < g^* - r^* < 0.1$ (dashed line) (cf. Fig. 2; this narrow range of $g^* - r^*$ color selects stars with similar effective temperature, ~ 7000–8000 K; Lenz et al. 1998) from the 90,569 stars shown in Figure 1a and for stars selected by the same criterion from the resulting sample of candidate RR Lyrae stars (solid line). The $u^* - g^*$ color of candidate RR Lyrae stars is 0.2 mag redder, on average, than that of nonvariable stars within the same narrow range of $g^* - r^*$ color. For main-sequence stars, the expected $u^* - g^*$ range is 0.85–1.0 (indicated as a horizontal line marked as $\log g = 4.5$ in the figure), and for horizontal-branch stars the expected $u^* - g^*$ range is 1.1–1.3 (horizontal line marked as $\log g = 2.5$), as found by Lenz et al. (1998). The intrinsic spread of the $u^* - g^*$ color for a given gravity is due to varying metallicity; the plotted values correspond to the range $-2.0 < [M/H] < 0$. The observed distribution of the $u^* - g^*$ colors of nonvariable stars is consistent with their being a mixture of low-gravity and high-gravity stars (for a detailed study of A stars detected in SDSS commissioning data, see Yanny et al. 2000a).

The number of candidates found here agrees within 1 σ with the normalization given by Wetterer & McGraw (1996). While this supports the low level of contamination by other types of variable stars, the large uncertainty of their normalization and our efficiency prevents an accurate determination of such contamination in our sample. As already discussed in § 3, our normalization assumes an efficiency for detecting RR Lyrae stars from two-epoch data of 56%, determined by the procedure described in the Appendix. This estimate agrees well with the efficiency determined from the comparison with the FASTT data (52% ± 15%). Another way to estimate efficiency is to compare the subsamples detected in the 20.9 deg^2 overlap of runs 77, 745, and 756. There are 41 candidates selected from runs 745 and 756, and 37 candidates from runs 77 and 745. These two subsamples have 16 sources in common, implying an efficiency of 41% ± 12%, in good agreement with the above estimates.

4.4. Light Curves for a Subsample of Candidate RR Lyrae Stars

The accepted identifying characteristics of an RR Lyrae star are its light curve and period. Here we present prelimi-
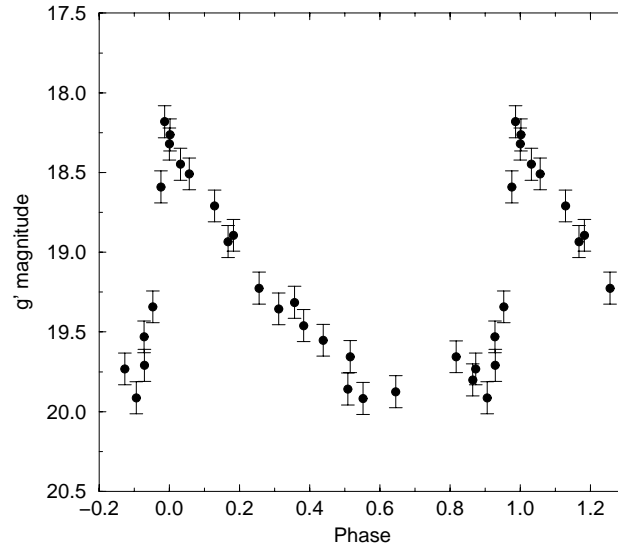
FIG. 11a
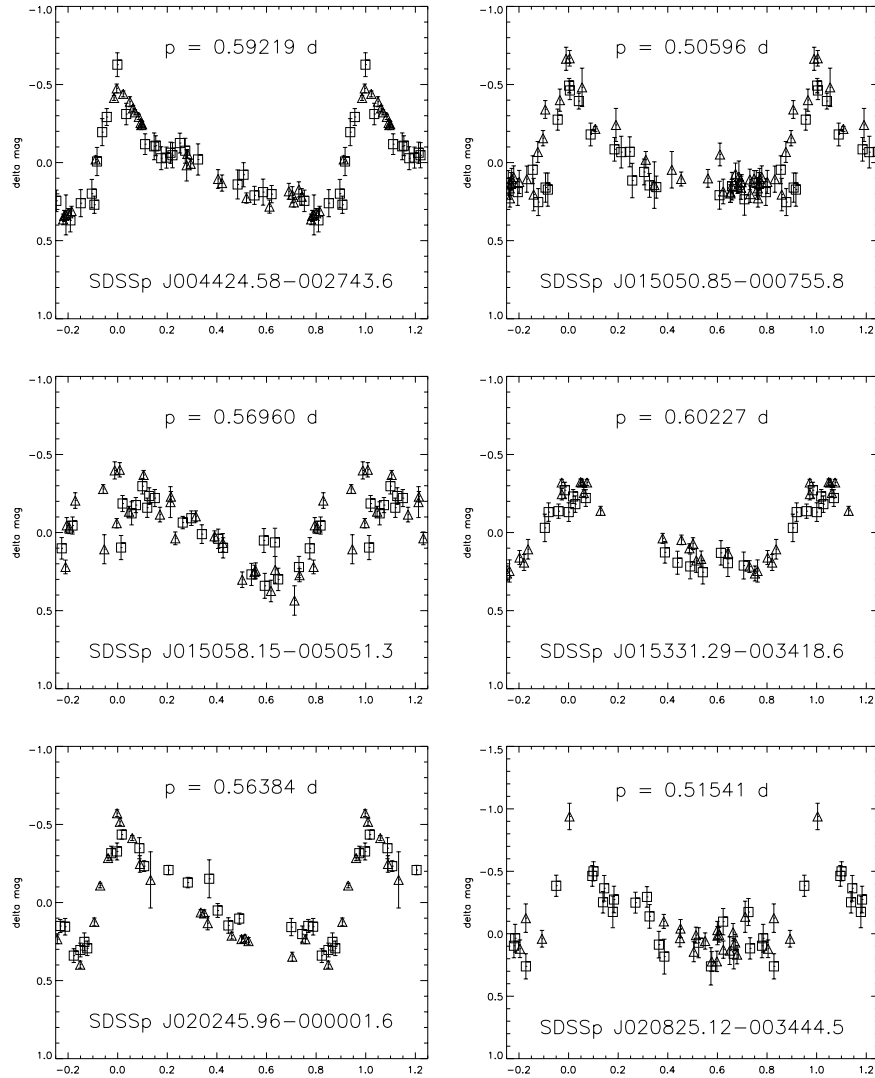
FIG. 11b

FIG. 11.—(a) Light curve in g′ band for SDSSp J113049.26−005918.2 obtained by the SDSS photometric telescope. The shape of the light curve and its period (0.46379 days) confirm that this candidate is an RR Lyrae star. (b) Johnson V-band light curves for six candidate RR Lyrae stars (not listed in Table 2) selected from SDSS commissioning data obtained in the southern Galactic hemisphere by the method described here. The light-curve data were obtained with the 0.76 m reflector of the University of Washington's Manastash Ridge Observatory (triangles) and supplemented by the data from the LONEOS database (squares). All six candidates have light curves with shapes and periods characteristic of RR Lyrae stars.

TABLE 2

No.	SDSS Name	HS Name[a]	g_1^*	r_1^*	g_2^*	r_2^*	$\langle r^* \rangle$[b]	$r_2^*-r_1^*$	$\langle g^*-r^* \rangle$[c]
1	SDSSp J104902.61+010500.6	...	17.66	17.38	16.75	16.78	17.08	−0.60	0.12
2	SDSSp J105314.69+011201.4	H01010306	14.77	14.75	14.53	14.55	14.65	−0.20	0.00
3	SDSSp J105926.11−005927.6	...	17.49	17.44	18.26	18.01	17.73	0.57	0.15
4	SDSSp J110035.99−003315.9	...	17.98	17.96	18.23	18.20	18.08	0.24	0.03
5	SDSSp J110838.26−000514.3	...	14.98	14.80	15.32	15.01	14.91	0.21	0.24
6	SDSSp J111010.79+010732.9	...	17.26	17.21	17.49	17.39	17.30	0.18	0.07
7	SDSSp J111705.98−003424.0	...	17.18	17.16	17.87	17.60	17.38	0.44	0.14
8	SDSSp J112425.37−000919.7	...	17.46	17.41	17.67	17.61	17.51	0.20	0.06
9	SDSSp J112837.73−000112.6	...	19.24	18.96	18.40	18.38	18.67	−0.58	0.15
10	SDSSp J113049.26−005918.2	...	19.84	19.63	18.92	18.92	19.27	−0.71	0.11
11	SDSSp J113814.16+010528.2	...	19.23	18.98	18.78	18.68	18.83	−0.30	0.18
12	SDSSp J114542.24+002314.6	...	17.59	17.43	17.96	17.67	17.55	0.24	0.22
13	SDSSp J114602.26+002057.7	...	20.25	20.00	19.52	19.54	19.77	−0.46	0.11
14	SDSSp J115113.99+004505.7	...	15.97	15.72	16.17	15.92	15.82	0.20	0.25
15	SDSSp J115534.40−003601.9	...	16.83	16.66	17.03	16.82	16.74	0.16	0.19
16	SDSSp J115628.60+011223.9	...	17.17	17.23	17.69	17.61	17.42	0.38	0.01
17	SDSSp J115706.95−005507.9	...	17.29	17.37	18.30	18.03	17.70	0.66	0.09
18	SDSSp J115724.21−005358.2	...	18.34	18.26	18.79	18.53	18.40	0.27	0.17
19	SDSSp J120047.92+004611.1	...	17.57	17.48	17.28	17.26	17.37	−0.22	0.05
20	SDSSp J120730.94−000412.6	...	16.97	16.95	17.81	17.60	17.27	0.65	0.12
21	SDSSp J121329.64−010151.9	...	17.46	17.32	17.74	17.51	17.41	0.19	0.19
22	SDSSp J121507.76+004930.1	...	17.70	17.72	18.16	18.08	17.90	0.36	0.03
23	SDSSp J121527.79−005256.5	...	15.50	15.54	16.59	16.40	15.97	0.86	0.08
24	SDSSp J121803.72+001448.9	...	18.60	18.34	17.86	17.86	18.10	−0.48	0.13
25	SDSSp J122228.39−010216.3	...	15.23	14.99	14.98	14.77	14.88	−0.22	0.23
26	SDSSp J122501.92+011407.9	I01010312	16.12	15.98	16.49	16.28	16.13	0.30	0.17
27	SDSSp J122529.03+011420.8	I01010394	15.39	15.40	15.91	15.70	15.55	0.30	0.10
28	SDSSp J123829.78+002001.6	...	18.51	18.54	18.98	18.90	18.72	0.36	0.03
29	SDSSp J124032.87−000312.9	...	17.51	17.19	17.25	16.99	17.09	−0.20	0.29
30	SDSSp J124046.56+005006.2	...	18.20	18.09	17.78	17.84	17.96	−0.25	0.03
31	SDSSp J124136.64+011306.5	...	17.15	17.09	17.56	17.31	17.20	0.22	0.15
32	SDSSp J124224.91−001203.1	I20060386	14.41	14.43	14.69	14.64	14.54	0.21	0.02
33	SDSSp J125028.28−000021.8	...	19.35	19.14	19.55	19.31	19.23	0.17	0.23
34	SDSSp J125208.73−002931.8	I28090270	15.61	15.44	16.05	15.83	15.63	0.39	0.20
35	SDSSp J125917.31+010240.4	...	19.57	19.25	18.81	18.78	19.02	−0.47	0.17
36	SDSSp J131045.97−002621.9	...	19.40	19.26	19.11	19.10	19.18	−0.16	0.07
37	SDSSp J131117.74−003429.9	...	15.05	15.11	15.96	15.75	15.43	0.64	0.08
38	SDSSp J131717.78−003558.0	...	19.08	18.92	18.84	18.71	18.82	−0.21	0.14
39	SDSSp J131757.46−000818.8	J21020002	17.40	17.15	17.02	16.91	17.03	−0.24	0.18
40	SDSSp J131806.63−003300.2	J29020030	15.88	15.87	16.10	16.06	15.96	0.19	0.03
41	SDSSp J132036.99+010945.4	...	18.68	18.72	19.40	19.15	18.93	0.43	0.11
42	SDSSp J132158.06+010659.3	...	18.96	18.99	19.16	19.14	19.06	0.15	0.00
43	SDSSp J132624.94−002612.1	J21040274	16.75	16.69	17.23	17.04	16.87	0.35	0.12
44	SDSSp J132635.08+002034.8	...	17.69	17.75	18.51	18.41	18.08	0.66	0.02
45	SDSSp J132700.05−005456.7	J37040583	15.29	15.04	14.84	14.80	14.92	−0.24	0.14
46	SDSSp J132745.54+001925.5	...	19.21	18.92	18.82	18.69	18.80	−0.23	0.21
47	SDSSp J133252.91+004622.6	J01060321	15.82	15.84	16.39	16.15	15.99	0.31	0.11
48	SDSSp J133323.47−001159.5	...	17.98	17.74	17.41	17.30	17.52	−0.44	0.18
49	SDSSp J133552.24−003706.8	J29070157	15.86	15.55	15.61	15.36	15.46	−0.19	0.28
50	SDSSp J133748.90−005646.6	...	19.45	19.19	18.82	18.81	19.00	−0.38	0.13
51	SDSSp J134142.51+004210.5	...	19.84	19.79	20.05	19.98	19.88	0.19	0.06
52	SDSSp J134452.37+003810.2	...	19.32	19.13	19.06	18.92	19.02	−0.21	0.16
53	SDSSp J134513.92+002240.0	...	17.00	17.08	17.31	17.32	17.20	0.24	−0.04
54	SDSSp J134521.33−000147.4	...	14.12	14.01	14.80	14.51	14.26	0.50	0.20
55	SDSSp J134529.59+002156.3	...	19.52	19.25	18.86	18.79	19.02	−0.46	0.17
56	SDSSp J134650.04+001659.7	...	18.96	18.91	18.45	18.54	18.73	−0.37	−0.02
57	SDSSp J134854.94+004622.4	...	19.29	19.20	18.81	18.84	19.02	−0.36	0.03
58	SDSSp J135007.45−005638.3	...	18.95	18.74	18.58	18.49	18.61	−0.25	0.15
59	SDSSp J135009.13−003414.3	...	15.60	15.66	16.61	16.38	16.02	0.72	0.09
60	SDSSp J135156.26−005314.2	...	18.96	18.85	19.20	19.00	18.93	0.15	0.15
61	SDSSp J135231.76+004350.9	...	17.48	17.45	18.22	17.99	17.72	0.54	0.13
62	SDSSp J135233.36−003336.9	...	19.36	19.17	19.57	19.36	19.27	0.19	0.20
63	SDSSp J135724.66−001028.9	...	19.07	19.05	19.27	19.23	19.14	0.18	0.03
64	SDSSp J135738.22+002055.6	...	19.08	18.83	18.78	18.63	18.73	−0.20	0.20
65	SDSSp J135824.04−002818.8	...	18.87	18.79	19.22	19.00	18.89	0.21	0.15

TABLE 2—*Continued*

No.	SDSS Name	HS Name[a]	g_1^*	r_1^*	g_2^*	r_2^*	$\langle r^*\rangle$[b]	$r_2^*-r_1^*$	$\langle g^*-r^*\rangle$[c]
66	SDSSp J135828.73+001248.5	...	19.09	18.81	18.60	18.49	18.65	−0.32	0.20
67	SDSSp J135955.38−002627.3	...	19.64	19.35	19.07	18.95	19.15	−0.40	0.21
68	SDSSp J140202.34+011243.5	...	20.02	19.90	19.62	19.59	19.74	−0.31	0.08
69	SDSSp J140206.54−002708.2	...	20.26	19.96	20.00	19.72	19.84	−0.24	0.29
70	SDSSp J140312.54+004802.7	...	19.33	19.08	19.57	19.28	19.18	0.20	0.27
71	SDSSp J140606.77−003356.8	...	15.58	15.35	15.74	15.50	15.43	0.15	0.23
72	SDSSp J140641.30+010818.1	...	19.60	19.34	19.11	18.97	19.16	−0.37	0.20
73	SDSSp J140829.95−003751.1	...	19.04	18.80	18.66	18.55	18.68	−0.25	0.18
74	SDSSp J140849.79−000422.2	...	19.15	18.97	19.41	19.18	19.07	0.21	0.21
75	SDSSp J141059.99−002916.3	...	19.12	19.11	19.60	19.40	19.25	0.29	0.11
76	SDSSp J141142.14+002248.5	...	16.41	16.13	15.86	15.73	15.93	−0.40	0.20
77	SDSSp J141238.55−005350.7	...	15.25	14.92	15.56	15.22	15.07	0.30	0.34
78	SDSSp J141446.16−002836.8	...	18.81	18.85	19.01	19.00	18.93	0.15	−0.02
79	SDSSp J141543.43−000613.0	...	16.85	16.66	17.22	16.97	16.81	0.31	0.22
80	SDSSp J141554.95+011003.4	...	19.67	19.44	19.36	19.23	19.34	−0.21	0.18
81	SDSSp J141724.61−000056.5	...	19.63	19.37	18.68	18.74	19.05	−0.63	0.10
82	SDSSp J141807.36+002302.6	...	15.33	15.10	14.92	14.81	14.96	−0.29	0.17
83	SDSSp J141846.15+010826.6	...	19.12	19.02	19.68	19.39	19.20	0.37	0.20
84	SDSSp J141858.06−002643.0	...	18.70	18.47	18.05	18.00	18.23	−0.47	0.14
85	SDSSp J141927.26+002215.7	...	19.83	19.53	19.60	19.37	19.45	−0.16	0.26
86	SDSSp J141934.16−005509.4	...	19.78	19.48	19.55	19.26	19.37	−0.22	0.29
87	SDSSp J142112.29+003936.3	...	19.52	19.12	18.86	18.79	18.95	−0.33	0.23
88	SDSSp J142257.47−002922.8	...	19.50	19.26	19.03	18.98	19.12	−0.28	0.14
89	SDSSp J142321.66−000705.1	...	19.33	19.29	20.01	19.78	19.54	0.49	0.14
90	SDSSp J142337.07+002502.7	...	19.54	19.42	19.85	19.67	19.55	0.25	0.15
91	SDSSp J142356.74−003428.5	...	16.35	16.19	15.99	15.95	16.07	−0.24	0.10
92	SDSSp J142502.47−005331.7	...	19.56	19.41	19.27	19.24	19.32	−0.17	0.09
93	SDSSp J142530.26−005153.8	...	19.59	19.28	18.80	18.74	19.01	−0.54	0.19
94	SDSSp J142602.36+010837.7	...	20.02	19.74	19.40	19.37	19.55	−0.37	0.16
95	SDSSp J142742.51−002848.8	...	19.56	19.27	18.43	18.50	18.88	−0.77	0.11
96	SDSSp J142807.14−000341.7	...	19.59	19.34	19.14	18.99	19.16	−0.35	0.20
97	SDSSp J142808.95−001148.3	...	16.51	16.34	16.09	16.12	16.23	−0.22	0.07
98	SDSSp J143032.31−000329.1	...	18.81	18.54	19.04	18.77	18.66	0.23	0.27
99	SDSSp J143241.74+001550.6	...	19.75	19.43	19.09	19.00	19.21	−0.43	0.21
100......	SDSSp J143311.76+011356.3	...	19.45	19.25	19.68	19.41	19.33	0.16	0.23
101......	SDSSp J143312.89−000733.5	...	19.52	19.30	19.07	19.04	19.17	−0.26	0.12
102......	SDSSp J143427.44−003721.2	...	19.01	19.02	19.35	19.28	19.15	0.26	0.03
103......	SDSSp J143614.78+010825.9	...	14.81	14.81	15.17	15.08	14.95	0.27	0.04
104......	SDSSp J143713.36+001623.0	...	15.72	15.71	16.09	15.87	15.79	0.16	0.12
105......	SDSSp J143924.18−003211.9	...	18.77	18.77	19.09	18.94	18.86	0.17	0.07
106......	SDSSp J144003.43+001346.4	...	19.64	19.53	20.02	19.78	19.66	0.25	0.17
107......	SDSSp J144424.47+010901.5	...	19.86	19.63	19.52	19.44	19.54	−0.19	0.15
108......	SDSSp J144427.84−005806.4	...	19.33	18.99	18.79	18.79	18.89	−0.20	0.17
109......	SDSSp J144618.52+001321.2	...	15.19	15.13	15.90	15.63	15.38	0.50	0.16
110......	SDSSp J144720.41−000101.7	...	17.94	17.63	17.55	17.35	17.49	−0.28	0.25
111......	SDSSp J144939.60−002943.9	...	16.80	16.79	17.61	17.35	17.07	0.56	0.13
112......	SDSSp J145258.17−000815.3	...	19.07	18.88	19.50	19.21	19.05	0.33	0.24
113......	SDSSp J145414.56+002310.3	...	19.83	19.52	18.91	18.90	19.21	−0.62	0.16
114......	SDSSp J145637.83−005622.8	...	18.88	18.92	19.88	19.61	19.27	0.69	0.11
115......	SDSSp J145719.71−005328.0	...	16.06	15.76	15.52	15.37	15.56	−0.39	0.22
116......	SDSSp J150129.25−005433.3	...	19.21	18.84	18.75	18.62	18.73	−0.22	0.25
117......	SDSSp J150147.85+004811.5	...	19.71	19.49	19.48	19.28	19.38	−0.21	0.21
118......	SDSSp J150218.16−000947.9	...	19.51	19.38	19.16	19.17	19.27	−0.21	0.06
119......	SDSSp J150257.73+001535.6	...	19.15	19.11	19.90	19.66	19.38	0.55	0.14
120......	SDSSp J150337.35−002812.8	...	14.98	14.77	15.24	14.98	14.88	0.21	0.23
121......	SDSSp J150545.38−000505.3	...	16.20	16.14	16.97	16.66	16.40	0.52	0.19
122......	SDSSp J150633.98+001806.6	...	17.49	17.42	17.79	17.71	17.57	0.29	0.07
123......	SDSSp J150807.79−000300.3	...	19.62	19.52	20.05	19.92	19.72	0.40	0.12
124......	SDSSp J150916.76+001947.2	K14010591	16.09	16.06	16.76	16.49	16.27	0.43	0.15
125......	SDSSp J151108.75−010015.2	...	19.72	19.46	18.81	18.89	19.18	−0.57	0.09
126......	SDSSp J151127.50−005511.9	...	19.56	19.54	19.98	19.87	19.70	0.33	0.07
127......	SDSSp J151216.31−003643.0	...	19.44	19.24	19.67	19.39	19.31	0.15	0.24
128......	SDSSp J151435.44−002959.7	K27030069	15.27	15.27	15.64	15.50	15.38	0.23	0.07
129......	SDSSp J151516.34−005124.2	...	19.96	19.65	19.67	19.41	19.53	−0.24	0.29
130......	SDSSp J151557.21−000653.2	...	17.47	17.44	17.73	17.61	17.52	0.17	0.08
131......	SDSSp J151610.53+011410.9	...	20.08	19.80	19.57	19.38	19.59	−0.42	0.23
132......	SDSSp J151659.66−005254.1	...	19.66	19.43	19.17	19.13	19.28	−0.30	0.13

TABLE 2—*Continued*

No.	SDSS Name	HS Name[a]	g_1^*	r_1^*	g_2^*	r_2^*	$\langle r^* \rangle$[b]	$r_2^* - r_1^*$	$\langle g^* - r^* \rangle$[c]
133......	SDSSp J151823.60+002122.2	...	17.70	17.42	17.35	17.27	17.34	−0.15	0.18
134......	SDSSp J152014.18−002603.0	K21041041	15.74	15.42	15.28	15.18	15.30	−0.24	0.21
135......	SDSSp J152122.93−000530.9	K21050106	17.06	17.10	17.90	17.60	17.35	0.50	0.13
136......	SDSSp J152132.05−010202.9	...	19.56	19.45	19.34	19.27	19.36	−0.18	0.09
137......	SDSSp J152318.61−005520.9	K34050625	16.87	16.50	17.09	16.72	16.61	0.22	0.37
138......	SDSSp J152547.10+002409.5	...	18.38	18.08	17.89	17.68	17.88	−0.40	0.25
139......	SDSSp J152711.10+002506.4	...	19.44	19.35	19.88	19.68	19.52	0.33	0.14
140......	SDSSp J152833.21−002546.9	...	19.83	19.66	19.58	19.48	19.57	−0.18	0.13
141......	SDSSp J153006.75+010806.7	...	20.02	19.75	19.49	19.33	19.54	−0.42	0.21
142......	SDSSp J153129.00+001724.5	...	19.89	19.53	19.04	19.05	19.29	−0.48	0.18
143......	SDSSp J153439.14−002615.4	...	19.24	19.09	19.52	19.30	19.20	0.21	0.18
144......	SDSSp J153443.29−002937.9	K27090033	15.57	15.46	16.15	15.82	15.64	0.36	0.22
145......	SDSSp J153502.96+001421.5	K14090198	16.00	15.86	15.61	15.61	15.73	−0.25	0.07
146......	SDSSp J153518.04+001405.9	...	17.65	17.32	17.30	17.11	17.21	−0.21	0.26
147......	SDSSp J153612.97+002039.5	...	19.26	19.17	19.45	19.34	19.26	0.17	0.10
148......	SDSSp J153938.01+011124.2	...	16.94	16.78	17.59	17.33	17.05	0.55	0.21

NOTE.—Positions are in J2000.0 coordinates; asinh magnitudes (Lupton, Gunn, & Szalay 1999) are quoted. For reference, zero flux corresponds to asinh magnitudes of 23.40, 24.22, 23.98, 23.51, and 21.83 in u^*, g^*, r^*, i^*, and z^*, respectively. Photometric errors are typically 0.03 mag (see § 2). Astrometric errors are typically 0″.1.

[a] Names from the Henden & Stone 1998 list (except for K14090198, which they discovered later from additional data).

[b] Mean r^* magnitude determined from two measurements.

[c] Mean $g^* - r^*$ color determined from the mean g^* and r^* magnitudes.

nary results of follow-up observations for several candidate RR Lyrae stars selected from SDSS commissioning data.

One of the faintest candidates in the sample, SDSSp J113049.26−005918.2 ($r^* \sim 19.4$), was monitored for five nights during 2000 March with the SDSS 20 inch (0.5 m) photometric telescope at Apache Point Observatory, New Mexico. Twenty-five individual measurements in g' band were taken over the five nights; the resulting light curve is shown in Figure 11a. The preliminary estimate for the period is 0.46379 days, and the first maximum is at HJD 2,451,606.2323. Both the light-curve shape and the period confirm that this candidate is a bona fide RR Lyrae star. The observed apparent magnitude of this star places it at ~ 55 kpc from the Galactic center, and at ~ 44 kpc from the Galactic plane.

Another sample of six candidate RR Lyrae stars was selected from SDSS commissioning data obtained in the southern Galactic hemisphere 59 days apart during the fall of 1998. While these data are not used in this work, the candidates were selected by identical procedures. The candidates were observed in the Johnson V band with the 0.76 m reflector of the University of Washington's Manastash Ridge Observatory during the fall of 1999. These observations were supplemented with data obtained from the LONEOS database, and the resulting light curves are shown in Figure 11b, together with the candidates' names and periods. All six candidates have light curves with shapes and periods characteristic of RR Lyrae stars. Their average Galactocentric distance is 30 kpc.

These prefatory follow-up observations show that the majority of stars in our sample are probably RR Lyrae stars, and they support the estimate that the contamination by other types of variable stars is $\lesssim 10\%$.

4.5. *Future Work*

These preliminary results obtained with a small sample of SDSS data indicate its potential for various Galactic structure studies. For example, the SDSS-FASTT and SDSS-LONEOS comparisons, and the light curves presented in

Figure 11, demonstrate that even two-epoch SDSS photometric data are sufficient for efficient detection of variable stars. The sample of candidate RR Lyrae stars presented here shows that such a deep and wide-area survey may significantly contribute to studies of the outer Galactic halo. Nevertheless, it is probable that this sample does not contain only RR Lyrae stars, and that some of the assumptions in our analysis may not be valid. The most straightforward approach to determine the contamination level by variables other than RR Lyrae stars is to obtain light curves for all candidates (so far only a few hundred, but over the next few years SDSS will produce several thousand candidate RR Lyrae stars). To facilitate such observations, Table 2 lists coordinates and two-epoch SDSS photometry in g' and r' bands for 148 candidates discussed in this work.[27] For the confirmed RR Lyrae stars, measurements of their radial velocity offer the exciting possibility of measuring the distribution of dark matter throughout the halo (Hawkins 1984).

---

[27] The finding charts are available from the authors upon request.

APPENDIX

MONTE CARLO STUDY OF THE SELECTION EFFECTS

To determine the sensitivity of the two-epoch selection of RR Lyrae stars presented in this work, we randomly sample a set of model light curves with realistic amplitude and period distributions. We use for this purpose a set of 180 RR Lyrae star light curves extensively measured by the ROTSE project,[28] as described by Akerlof et al. (2000). Spline fits to these phased light curves provide our templates.

For each template object, we sample the light curve at two points separated by the nominal 1.99462 day spacing for 1000 random phases. Because this spacing is at least 3 times longer than typical RR Lyrae star periods ($\lesssim 0.7$ days), the details of the adopted period distribution have only a minor impact on the model results. For the same reason, stars with periods shorter than RR Lyrae periods (e.g., SX Phoenicis stars) are selected with roughly the same efficiency. For each sampling, we obtain a real magnitude difference, apply SDSS photometric errors to the two "measurements," and determine whether this object would pass our variability selection criteria. This allows us to realistically assess our efficiency as a function of magnitude. In addition, it allows us to characterize the effect of two-epoch observations on our observed mean magnitudes and, hence, on distance estimates.

We find that at bright magnitudes, the detection efficiency is constant at the level of 56%, which is imposed by the combination of the two-epoch selection and RR Lyrae light-curve shapes. The efficiency falls off slowly beginning at $r* \sim 19$ because of increased photometric errors and is reduced to half its peak value at $r* \sim 20$. We also find that the mean magnitudes calculated from two-epoch data are biased toward the bright side for about 0.1 mag, because the RR Lyrae light curves are not symmetric around the mean brightness. The mean rms deviation of RR Lyrae light curves used in this analysis is 0.21 mag and is practically independent of the number of epochs as long as it exceeds ~ 10. We note that the light curves used in this analysis were obtained with an open CCD and thus are representative of the red bands. Because of this effect, the RR Lyrae amplitudes in bluer bands (e.g., g' and r') may be somewhat larger, and we adopt a conservative upper limit of 0.3 mag used in the comparison with the FASTT data (§ 4.1).

---

[28] See http://www.umich.edu/~rotse.

REFERENCES

Abell, G. O. 1955, PASP, 67, 258
Akerlof, C., et al. 2000, AJ, 119, 1901
Annis, J., et al. 2000, in preparation
Doi, M., et al. 2000, in preparation
Fan, X. 1999, AJ, 117, 2528
Fan, X., et al. 1999, AJ, 118, 1
Fukugita, M., Ichikawa, T., Gunn, J. E., Doi, M., Shimasaku, K., & Schneider, D. P. 1996, AJ, 111, 1748
Guhathakurta, P., Yanny, B., Bahcall, J. N., & Schneider, D. P. 1994, AJ, 108, 1786
Gunn, J. E., et al. 1998, AJ, 116, 3040
Gunn, J. E., & Weinberg, D. H. 1995, in Wide Field Spectroscopy and the Distant Universe, ed. S. J. Maddox & Aragón-Salamanca (Singapore: World Sci.), 3
Harris, H. C. 1993, AJ, 106, 604
Hartwick, F. D. A. 2000, AJ, 119, 2248
Hawkins, M. R. S. 1984, MNRAS, 206, 433
Henden, A. A., & Stone, R. C. 1998, AJ, 115, 296
Hoffmeister, C., Richter, G., & Wenzel, W. 1985, Variable Stars (New York: Springer)
Ibata, R. A., Lewis, G. F., Irwin, M., Totten, E., & Quinn, T. 2000, ApJ, submitted (astro-ph/0004011)
Ibata, R. A., Wyse, R. F. G., Gilmore, G., Irwin, M. J., & Suntzeff, N. B. 1997, AJ, 113, 634
Johnston, K. V., & Majewski, S. R., Siegel, M. H., Reid, I. N., & Kunkel, W. E. 1999, AJ, 118, 1719
Johnston, K. V., Zhao, H., Spergel, D. N., & Hernquist, L. 1999, ApJ, 512, L109
Kent, S. M., et al. 2000, in preparation

Krisciunas, K., Margon, B., & Szkody, P. 1998, PASP, 110, 1342
Layden, A. C., Hanson, R. B., Hawley, S. L., Klemola, A. R., & Hanley, C. J. 1996, AJ, 112, 2110
Lenz, D. D., Newberg, J., Rosner, R., Richards, G. T., & Stoughton, C. 1998, ApJS, 119, 121
Lupton, R. H., Gunn, J. E., & Szalay, A. S. 1999, AJ, 118, 1406
Lupton, R. H., et al. 2000, in preparation
Margon, B., & Deutsch, E. W. 1999, PASP, 111, 45
Oke, J. B., Giver, L. P., & Searle, L. 1962, ApJ, 136, 393
Oke, J. B., & Gunn, J. E. 1983, ApJ, 266, 713
Petravick, D., et al. 1994, Proc. SPIE, 2198, 935
Pier, J. R. 1983, ApJS, 53, 791
Pier, J. R., et al. 2000, in preparation
Preston, G. W. 1959, ApJ, 130, 507
Rosino, L. 1951, Mem. Soc. Astron. Italiana, 22, 309
Saha, A. 1984, ApJ, 283, 580
Schlegel, D. J., Finkbeiner, D. P., & Davis, M. 1998, ApJ, 500, 525
Siegmund, W., et al. 2000, in preparation
Smith, G. H., McClure, R. D., Stetson, P. B., Hesser, J. E., & Bell, R. A. 1986, AJ, 91, 842
Smith, H. A. 1995, RR Lyrae Stars (Cambridge: Cambridge Univ. Press)
Smith, J. A., et al. 2000, in preparation
Uomoto, A., et al. 2000, in preparation
Tucker, D. L., et al. 2000, in preparation
Wetterer, C. J., & McGraw, J. T. 1996, AJ, 112, 1046
Wilson, A. G. 1955, PASP, 67, 27
Yanny, B., et al. 2000a, ApJ, in press
————. 2000b, in preparation
York, D. G., et al. 2000, AJ, in press